ADVANCED OPTICAL MATERIALS

Supporting Information

for *Advanced Optical Materials,* DOI: 10.1002/adom.201801214

A Reconfigurable Color Reflector by Selective Phase Change of GeTe in a Multilayer Structure

Mohsen Jafari, L. Jay Guo,* and Mina Rais-Zadeh*

Supporting Information

DOI: 10.1002/ ((please add manuscript number))
Article type: Full Paper

A reconfigurable color reflector by selective transitioning of a phase change material in a multi-layer structure

Mohsen Jafari[1], L. Jay Guo*[1], and Mina Rais-Zadeh[1,2]
Mohsen Jafari, Prof. Jay Guo
Department of Electrical Engineering and Computer Science, University of Michigan, Ann Arbor, MI, USA.
E-mail: guo@umich.edu
Prof. Mina Rais-Zadeh
NASA Jet Propulsion Laboratory, California Institute of Technology, Pasadena, CA, USA

Keywords: Fabry-Pérot Cavity, Germanium Telluride, Optical Switch, Phase Change Material, Color Filter

Abstract-This document provides supplementary information to, "A reconfigurable color reflector by selective transitioning of a phase change material in a multi-layer structure". Within this document, design and methods are discussed in greater detail, and an in-depth discussion of the finite element method (FEM) is presented to further the understanding of the tunable color reflector operation within the visible region. To quantitatively compare the reflected color of the device, the International Commission on Illumination (CIE) standard was used. This supplementary document discusses the CIE standard's specification and derivation of color graphs to demonstrate the dynamic range of colors achieved in this research. Furthermore, device fabrication, including greater specification of the relevant processes, is explained. Finally, device reliability is studied by applying several hundreds of voltage pulses with no significant change in the reflected color.

1. Introduction:

The main part of this supplementary document presents the design challenges encountered when using a phase change material (PCM) in visible wavelengths, as PCMs are generally very lossy in this

region. In the main document we presented a design which incorporated Germanium Telluride (GeTe) due to its well-understood stoichiometry and more desirable chemical properties compared to that of the more complex and common compound, Germanium Antimony Telluride (GeSbTe or GST). Compared to GST, use of GeTe produces more reliable devices with higher thermal budgets through a much simpler and CMOS-compatible fabrication processes. To address the challenge of GeTe high loss in the visible range, we incorporated a novel design approach that improves the modulation index by enhancing the reflected signal sensitivity to the change in the refractive index of GeTe during phase transition.

The design properties can be further characterized in the context of the wide window of absorption that the device structure supports within the visible spectrum (380 nm-750 nm). The unique structural design enhances the sensitivity of the light reflection and the optical index modulation using multiple ultra-thin GeTe films integrated in this layered media. Multiple ultra-thin GeTe films create spatially separated nodes for the electromagnetic waves which filter either the blue or red region of the visible wavelength depending on the crystallographic phases of each layer.

The extraction of quantitative values to represent the colors, which are visible to human eyes is discussed using the CIE standard.[1] The design process includes a number of weight functions which are provided by the standards. The consideration of the weight functions yields a larger range of dynamic colors when GeTe layers complete crystallographic phase transitions. Furthermore, the realization of selective phase transitioning of each specific layer within the same device, using only a single heater, has proven to be reliable through several hundred switching events.

2. Modeling and Methods:

2.1. Electromagnetics FEM modeling:

In this section, the electromagnetic response of the device is discussed using FEM modeling (COMOSL Multiphysics ®).[2] Device reflection spectra in each of the four different states are shown in Figure S. 1. Both reflection and absorption are shown for each of these four states. As shown below,

the device supports a wide absorption in the 450 nm to 675 nm range. This wide range of absorption is created by the thin film resonance located at these two wavelengths. The wide absorption window, which is located exactly at the edge of blue and red colors, increases the device color sensitivity to modulation of GeTe refractive index by the tuning of two ultra-thin GeTe films integrated in the structure. The reflection peak located at 550 nm appears when the bottom GeTe layer is amorphous and is not dependent upon the phase of the top layer. In the amorphous state light propagates through the optical phase shift layer between the bottom GeTe layer and bottom reflector of the cavity (Fig. 2(a)). The reflected light is green in color when the top GeTe layer is crystalline and absorbs most of the red color. This green color is most visible when the bottom layer is amorphous. When both top and bottom films are amorphous, a large reflection of red color is produced. The peak located at 380 nm is fixed within the structure and provides reflection of blue color, which is only visible when both films are crystalline and are absorbing the remainder of the spectrum as shown in the first state. The electric and magnetic fields of these different modes are shown in Figure S. 2 for different wavelengths in visible range.

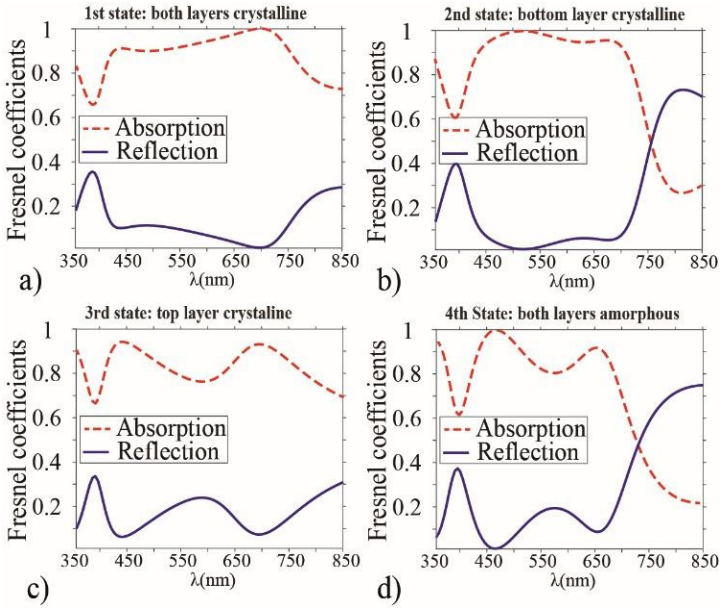

Figure S. 1. Theoretical modeling of absorption and reflection spectra for four different states of the device in the visible range.

As shown in Figure S. 2(c), for an effective reflection of red color, the structure must support a peak in electric field at the position of the top GeTe layer. The absence of properties necessary to support a peak when the top layer is crystalline (first and third states) diminishes the red color reflection from ~70 % to 30 %. This decrease produces majority blue and green colors in these two states with a top layer that is in the crystalline phase. The green colors are most easily seen by a human eye due to greater sensitivity of green cone cells, as further explained in the next section.

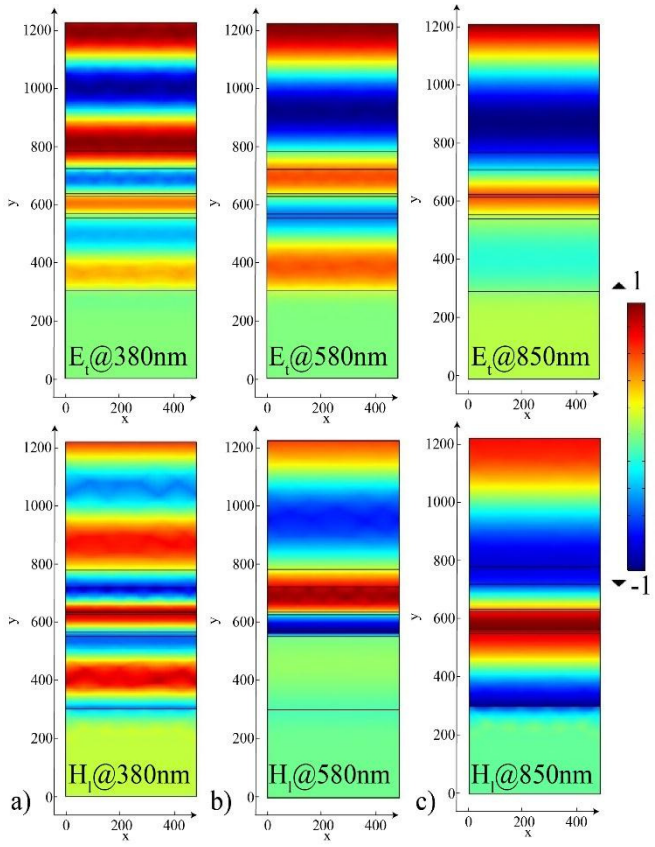

Figure S. 2. Patterns of normalized electric (top) and magnetic (bottom) fields shown for the cross-section of the device at wavelength of 380 nm (a), 580 nm(b), and 850 nm(c); blue (red) regions represent the fields' minima (maxima) when GeTe films are amorphous.

2.2. Thermal Modeling

To demonstrate the selective transitioing of GeTe films within the stack using joule heating a thermal model is studied employing FEM. Temperature dependent densities, heat capacities, and

thermal conductivities measured/estimated experimentally[3,4] were incorporated into the model for crystalline and amorphous states. Figure S. 3 shows the required temperature distribution within the stack in order to achieve four different states mentioned in the main paper. Slow CA pulse with 1 µs pulse width and 200 nm rise and fall times heats the whole stack to 175 °C which only transitions the top thick layer; the fast CA pulse with 50 ns rise time and 500 ns duration heats the bottom layer to 183 °C and crystalize it. The top GeTe layer is kept at 166 °C well below its Tx in the amorphous state. The CC state is achieved by a slow 1 µs pulse and higher amplitude to heat up the whole stack to 186 above Tx of both GeTe layers.

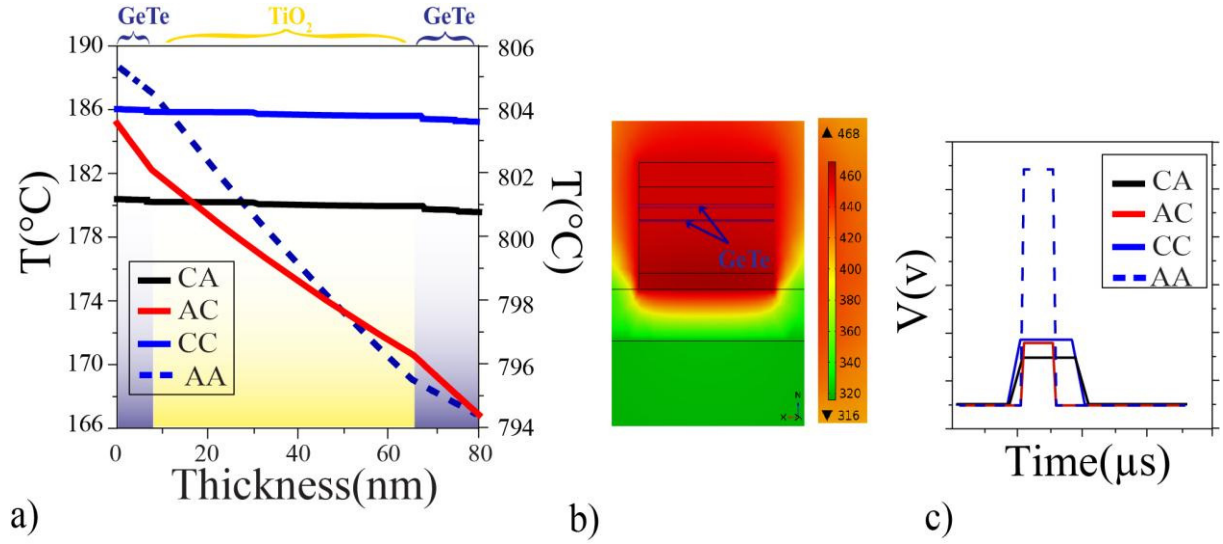

Figure S. 3. Temperature profile versus thickness within the stack of the films between two GeTe films (b) Temperature profile within the stack for AC state. (c) Four differetn voltage pulese used to achieve AA (a), AC (b), CA (c), and (CC) states (the vales are not to scale).

These temperature profiles were achieved by applying the voltage pulses across the Pd heater underneath the stack of the films. Different pulses used to achieve AA, AC, CA, and CC states are also demonstrated in Figure S. 3 (c).

2.3. CIE chromaticity graph extraction:

Device reflection spectra were extracted using an ellipsometer for visible-NIR regions. Device reflection is extracted from the measured value of the Φ and Δ parameters at different angles ranging from 45° to 75°. To determine the actual color seen from these reflection spectra, a common CIE

1931-2° standard is used.[2,5] Typical human eyes have three different types of cone cells located inside the fovea that perceive the colors mostly around 2° arc. Normalized spectral sensitivities of these three types of cone cells (S, M, and L) are extracted for a CIE standard observer. Three standard observer color matching functions are then derived from these sensitivities which are defined as: $\bar{x}(\lambda)$, $\bar{y}(\lambda)$, and $\bar{z}(\lambda)$ (Figure S. 4).

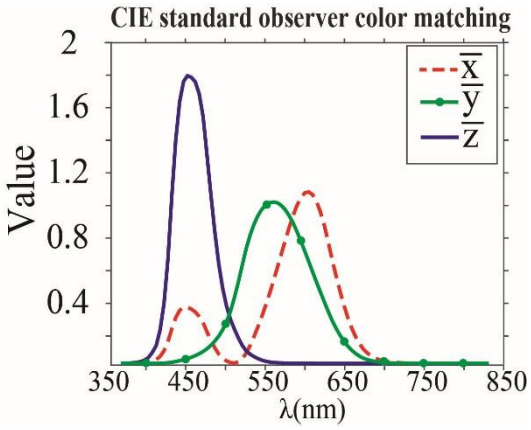

Figure S. 4.CIE color matching function obtained for the standard observer for the sensitive 2º arc inside fovea.

These matching functions are then integrated over the visible spectrum (390 nm-830 nm) and multiplied by the sample's measured reflection times spectral power distribution of the illuminant to determine X, Y and Z as following:

$$\mathbf{X} = \frac{\mathbf{K}}{\mathbf{N}} \int \mathbf{R}(\boldsymbol{\lambda}) \times \mathbf{I}(\boldsymbol{\lambda}) \times \bar{\mathbf{x}}(\boldsymbol{\lambda}) \mathbf{d}\boldsymbol{\lambda} \quad \textbf{(S1)}$$

$$\mathbf{Y} = \frac{\mathbf{K}}{\mathbf{N}} \int \mathbf{R}(\boldsymbol{\lambda}) \times \mathbf{I}(\boldsymbol{\lambda}) \times \bar{\mathbf{y}}(\boldsymbol{\lambda}) \mathbf{d}\boldsymbol{\lambda} \quad \textbf{(S2)}$$

$$\mathbf{Z} = \frac{\mathbf{K}}{\mathbf{N}} \int \mathbf{R}(\boldsymbol{\lambda}) \times \mathbf{I}(\boldsymbol{\lambda}) \times \bar{\mathbf{z}}(\boldsymbol{\lambda}) \mathbf{d}\boldsymbol{\lambda} \quad \textbf{(S3)}$$

where K is a scaling factor and N is:

$$\mathbf{N} = \int \mathbf{I}(\boldsymbol{\lambda}) \times \bar{\mathbf{y}}(\boldsymbol{\lambda}) \mathbf{d}\boldsymbol{\lambda} \quad \textbf{(S4)}$$

X, Y, and Z are calculated from these integrals and used to define the normalized chromaticity coordinates x and y, as well as the brightness or luminance of the color (Y). These set of two

coordinates (x,y) and their brightness (Y) are enough to show all colors human eyes can sense with its three types of cone cells. These coordinates are defined as:

$$\mathbf{x} = \frac{\mathbf{X}}{\mathbf{X+Y+Z}} \quad \textbf{(S5)}$$

$$\mathbf{y} = \frac{\mathbf{Y}}{\mathbf{X+Y+Z}} \quad \textbf{(S6)}$$

These coordinates are used to locate the actual reflected color of the sample as shown in Figure 6 of the main article for the brightest colors (i.e. maximum Y). Numbers on the outer curve boundary show the wavelengths of monochromatic light reflection. It is also important to note that colors, which are seen in this figure and all other CIE graphs, depend on the display or printer RGB calibration as well as other specifications.

Fabrication:

The fabrication process starts with a single-side polished silicon wafer. A 100 nm thick palladium film with a 10 nm NiCr adhesion layer was evaporated and patterned using the lift-off process. The SiO_2 optical phase-shift layer was then deposited using a PECVD tool (Plasma-Therm Co.) at 200 ºC with a rate of 7.5 Å/sec. Then a 15 nm GeTe film was sputtered in a deposition system (Kurt J. Lesker® Co.) from a 3-inch $Ge_{50}Te_{50}$ target (Mitsubishi Material Co.) using Ar^+ carriers with a rate of 0.66 Å/sec at room temperature. An ultra-low sputtering rate was used to improve the film uniformity and obtain an optical loss close to bulk value in the as-sputtered amorphous films. The TiO_2 separators were evaporated using SJ-20 evaporators at room temperature and 2×10^{-6} torr chamber pressure. An antireflection coating consisting of MgF_2 film was also evaporated using the same SJ-20 evaporated with an ultra-low deposition rate of 0.4 Å/sec. MgF_2 deposition parameters were tuned to achieve a stable, low-loss and low-stress film at room temperature. The fabrication is shown in Figure S. 5.

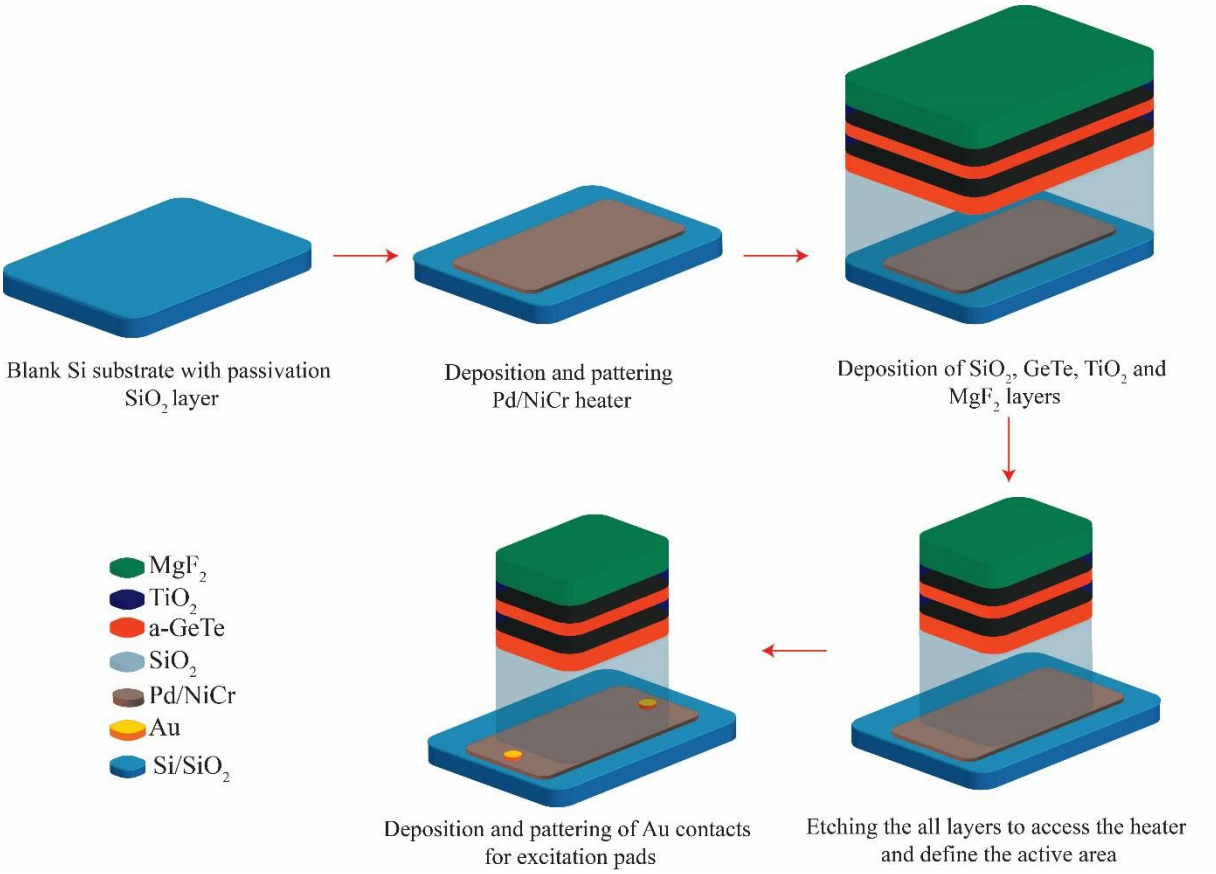

Figure S. 5. Fabrication process used to implement the tunable color reflector.

3. Results and test:

The reliability of the color reflector is an important factor in its long-term performance. The device under test (DUT) was connected to a pulse generator to simulate accelerated aging. Several hundreds of pulses were applied to the device and the color tunability of the device was analyzed after testing using ellipsometer spectroscopy. The (x,y) coordinates of the samples after different numbers of applied pulses are shown in Figure S. 6. As shown below, the device performance remains the same after hundreds of pulses are applied to it. "X" and "Y" coordinates did not show much variation, even after 200 pulses were applied to the heater for each of the four different states (800 pulses total). The bottom layer was crystallized with the application of 0.9 V and the top layer was crystallized with the application of 1.2 V. The reset pulses were applied to the device with the magnitude of 6.5 V. The heater was also tested and found to tolerate 20 V high voltage operation before any device failure occurs.

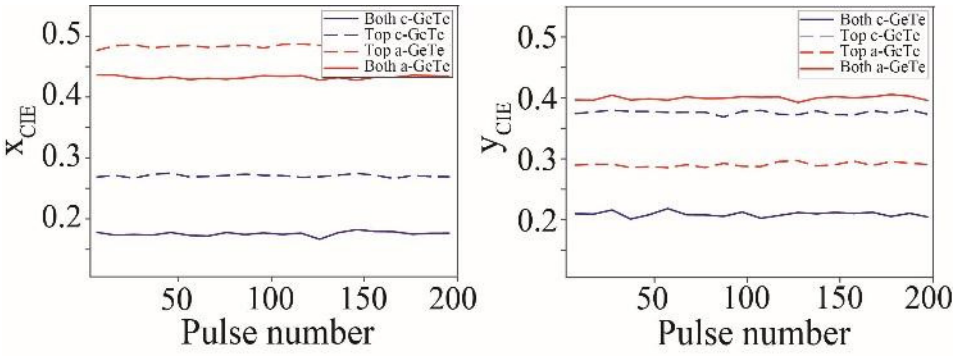

Figure S. 6. CIE specification variation versus number of pulses shown for X coordinates (left) and Y coordinates (right) for up to 200 pulses.

Conclusion

This document is presented as supplementary material to further explain the selective phase transition obtained through the use of multiple GeTe layers in a color reflector by providing additional information on the design, fabrication, and measurements. Additionally, it includes a discussion of the basic idea behind the design and the fabricated device reliability during multiple switching events. It is the intention of this supplementary document to support and further explain the results and procedures presented in the main article entitled, "A reconfigurable color reflector by selective transitioning of a phase change material in a multi-layer structure".

References

1. CIE (1932). Commission internationale de l'Eclairage proceedings, 1931. Cambridge: Cambridge University Press.
2. COMSOL Multiphysics® v. 5.2. www.comsol.com. COMSOL AB, Stockholm, Sweden.
3. Chopra, K. L., and S. K. Bahl. "Amorphous versus crystalline GeTe films. I. Growth and structural behavior." Journal of Applied Physics 40.10 (1969): 4171-4178.
4. Liu, Jie, et al. "A multi-scale analysis of the crystallization of amorphous germanium telluride using ab initio simulations and classical crystallization theory." Journal of Applied Physics 115.2 (2014): 023513.
5. T. Smith, J. Guild, Trans. Opt. Soc **1931**, 33(3), 73.